Finned, Multibody Aerodynamic Interference at Transonic Mach Numbers

Charles J. Cottrell* and Lawrence E. Lijewski†
U. S. Air Force Armament Laboratory, Eglin Air Force Base, Florida

A wind tunnel experiment involving single, double, and triple combinations of mutually interfering, generic, finned aircraft stores has been conducted. Each combination of stores was tested at Mach numbers from 0.60 to 1.20, at angles of attack from 0 to 20 deg for the single store, and from 0 to 10 deg for the double- and triple-store configurations. Extensive body and fin pressure and flow visualization data were obtained at each store location. The data indicate that finned, multibody interference (measured on the body) in the transonic region seems to be greatest at Mach numbers near 1, and subsides as the freestream Mach number increases or decreases from sonic conditions. Although somewhat dependent on fin orientation, the inboard fins seem to experience greater multibody interference at $M_\infty = 0.60$ than at Mach numbers closer to 1. An Euler solution for the double-store configuration (x fin orientation) at $M_\infty = 0.95$, 0 deg angle of attack was generated and compared with these data. The generally good correlation indicates that an Euler flow solver can yield accurate predictions of the location and magnitude of multibody interference on both the body and the fins, provided the viscous effects associated with these configurations remain small.

Nomenclature

C_p = pressure coefficient $(P-P_\infty)/(\frac{1}{2}\rho_\infty V_\infty^2)$
C_p^* = pressure coefficient for Mach number = 1
L = model length, 30.18 cm (11.88 in.)
L_c = local fin chord length
M_∞ = freestream Mach number
P = static pressure
P_∞ = freestream static pressure
V_∞ = freestream velocity
X = model axial location measured from nose tip
XF = location along the local chord L aft of the leading edge
α = angle of attack
η = fin spanwise location
ρ_∞ = freestream density
ϕ = body circumferential angle
ϕ_f = fin orientation angle

Introduction

IT is widely recognized that the speed, range, and endurance of fighter aircraft can be influenced by the aerodynamic forces generated by mutually interfering stores in external carriage.[1] It is difficult to predict these forces numerically, particularly in the transonic Mach range where embedded regions of subsonic and supersonic flow preclude the use of marching codes. However, recent advances in high-speed, large-memory supercomputers permit the use of Euler and Navier-Stokes flow solvers to investigate the flow interactions that occur around multibody configurations. The use of these flow solvers to predict forces and moments accurately is increasing at a fast pace.[2-4]

A comprehensive experimental data base is required to guide and verify these efforts in computational fluid dynamics (CFD). Unfortunately, existing data often are not of a generic nature and may involve geometric complexities that render them unsuitable for influencing the step-by-step evolution of CFD codes and algorithms. To satisfy this need partially, a series of wind tunnel experiments is being conducted to acquire pressure and flow visualization data around mutually interfering, generic-shaped stores in multiple-component configurations both inside and outside the vicinity of a fighter-like fuselage or wing. Results of the first wind tunnel experiment, which involved mutually interfering, unfinned bodies of revolution, are reported in Ref. 5.

The purpose of this paper is to extend that previous study by encompassing finned bodies in mutually interfering, multicomponent configurations. This will be accomplished by using a portion of the recent experimental results along with Euler flow solver predictions to study mutual aerodynamic interference involving two and three finned-store combinations at transonic conditions. Although no rack is included in these configurations, it is recognized that its presence would significantly effect the flowfield and, hence, the store loads.[6] This present study is a first step toward the computational analysis of loads acting on a store in a real rack-carriage configuration.

Model and Test Conditions

The experiment was conducted in the Arnold Engineering Development Center PWT-4T wind tunnel. The model consisted of one-, two-, and three-store combinations of a 2-in.-diam generic store consisting of a 3.333 caliber cylindrical centerbody and a 1.667 caliber tangent ogive forebody and afterbody, with the afterbody truncated to mount to a sting. The model had four low aspect ratio fins. Each of these cruciform fins had the cross section of a NACA 0008 airfoil. Details of the model are presented in Fig. 1a. The distance between the stores was 0.80 fuselage diameter for both the two- and three-body configurations (Fig. 1b). Only one store was

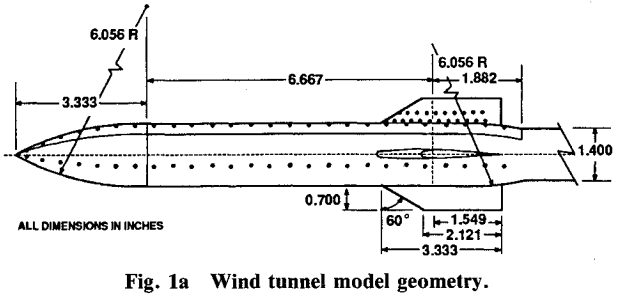

Fig. 1a Wind tunnel model geometry.

Presented as Paper 87-2480 at the AIAA 5th Applied Aerodynamics Conference, Monterey, CA, Aug. 17-19, 1987; received Sept. 11, 1987; revision received Dec. 1, 1987.

*Chief, Plans and Programs Office, Aeromechanics Division. Senior Member AIAA.

†Research Scientist, Computational Fluid Dynamics Section, Aerodynamics Branch, Aeromechanics Division. Senior Member AIAA.

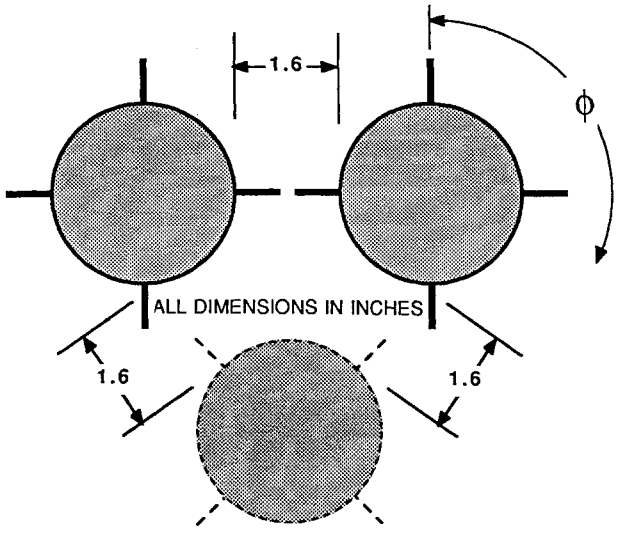

Fig. 1b Two- and three-store configuration alignment (+ fin orientation).

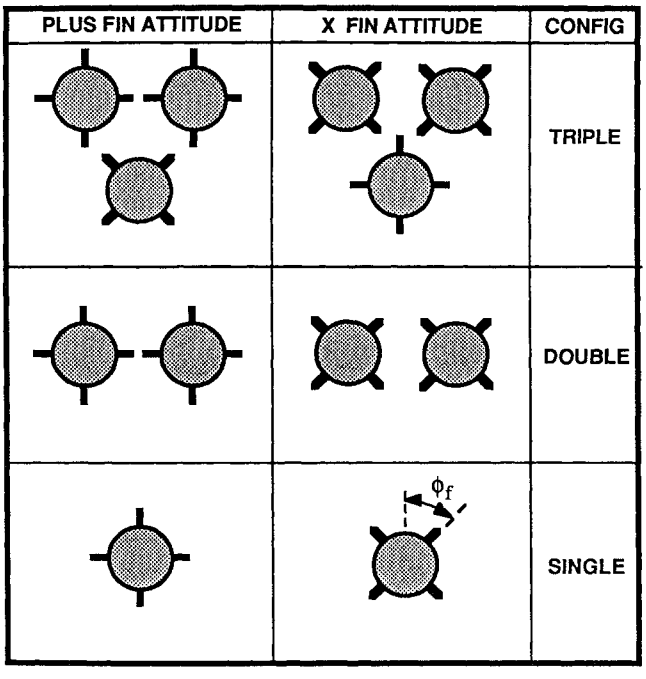

Fig. 1c Store configurations.

instrumented. It contained a total of 198 pressure taps. There were 116 taps situated in four rows of 29 orifices along the length of the body. These four rows were, respectively, located at 10, 20, 30, and 40 deg (clockwise looking downstream) from each fin centerline. Also, there were chordwise rows of 8 to 13 orifices at eight spanwise locations on the fins (two rows per fin).

The six test configurations are shown in Fig. 1c. These include both + (plus) and x fin alignments for the single, double, and triple configurations. Note that the bottom store fin orientations for the triple configurations are opposite those of the shoulder stores. This was done to reflect more accurately a general characteristic of wing-mounted store loadings on a fighter aircraft.

The instrumented store was rotated to measure body pressure at 10 deg intervals around its circumference from each configuration. However, no body pressure data were obtained at $\phi = 0$, 90, 180, or 270 deg because of model design constraints. In addition, the instrumented store was rotated to measure fin pressure at $\phi_f = 0$, 90, 180, and 270 deg and at $\phi_f = 45$, 135, 225, and 315 deg for + and x fin attitudes, respectively. The instrumented model was repositioned to record similarly pressure data at each store position in the two- and three-body configurations. Details of the three-body (+ fin) configuration mounted in the wind tunnel test section are shown in Fig. 2.

Each configuration was tested at $M_\infty = 0.60$, 0.80, 0.95, 1.05, and 1.20 with a freestream unit Reynolds number maintained at approximately 2.4×10^6/ft for all cases. Every configuration was tested at angles of attack α equal to 0, 2, 4, 6, and 10 deg. In addition, the single-store configurations were tested at $\alpha = 15$ and 20 deg. Oil flow visualization photographs were obtained following acquisition of the pressure data.

Euler Flow Solver

An Euler solver[7] was used to predict the pressure distributions on the double-store (x fin) configuration at 0 deg angle of attack. The solver uses an implicit, two-pass upwind scheme[8] and is second-order accurate in space. It solves the flux-vector-split form of the Euler equations and is stable for a wide range of Courant numbers for steady-state computations. The Euler equations are written in strong conservation law form in order to capture discontinuities in the flow such as shocks. The scheme uses a finite-volume formulation in order to achieve total flexibility with regard to geometry. Local time stepping is used to accelerate convergence for steady-state problems. The code has a multiblock capability to allow calculations of finned bodies at angle of attack. Characteristic variable boundary conditions[9] are used by the solver on far-field boundaries and at the body surfaces.

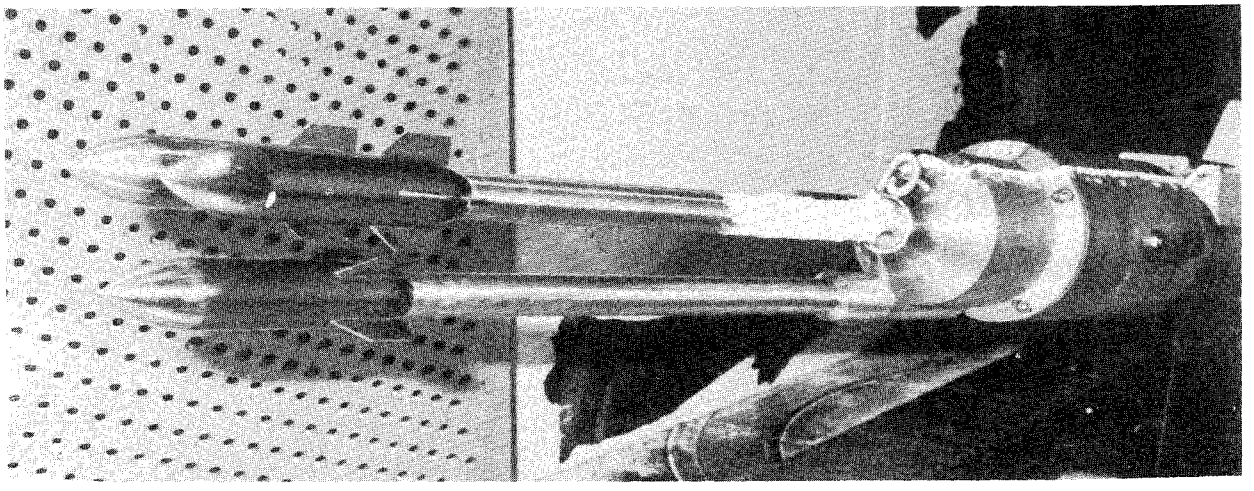

Fig. 2 Three-store (+ configuration) model installation.

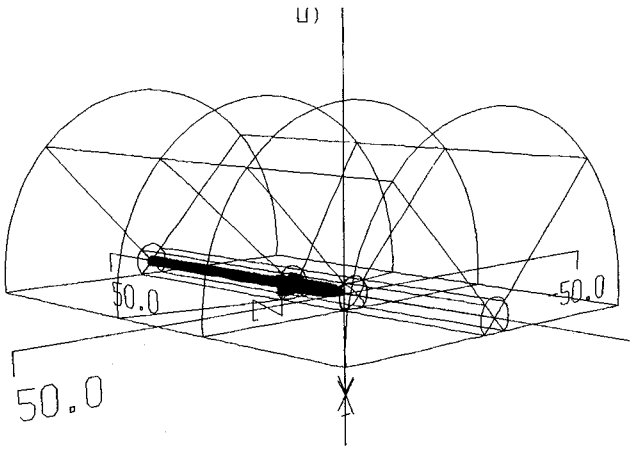

Fig. 3a Wire frame of computational multiblock region with embedded surface grid.

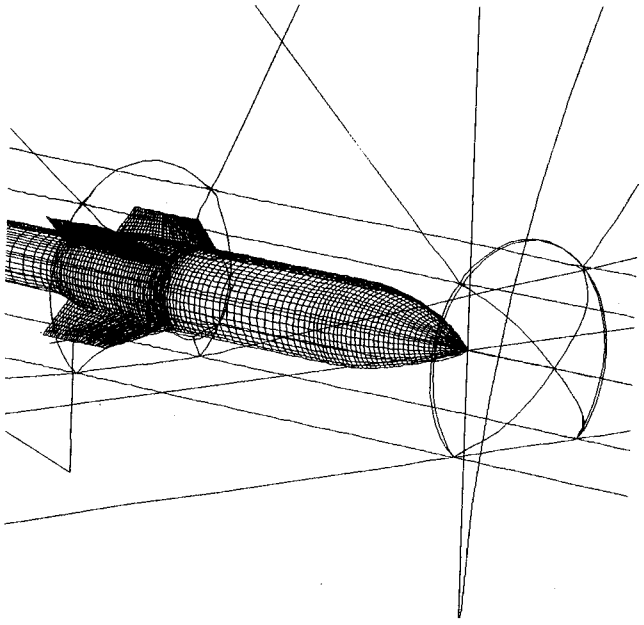

Fig. 3b Closeup of embedded finned body surface grid.

Computational Grid

To obtain an accurate flow solution, a smooth grid must be generated on which to solve the fluid flow equations. The elliptic grid generation method chosen was developed by Thompson and Warsi.[10] The grid generation scheme uses boundary-conforming coordinate systems to treat boundaries of arbitrary shape. Control of the grid line spacing and orientation in the field are achieved by adopting a system of Poisson-like equations. For complex, three-dimensional configurations, it is often difficult to obtain a reasonable grid with the entire physical region transformed into a single, rectangular computational space. The preferred approach is to segment the physical region into continuous subregions bounded by six curved surfaces, with each subregion transformed into a rectangular computational block. An individual grid is generated in each subregion and then patched together to form the overall grid. For the two-body, x-fin configuration, 21 subregion grids were generated around one finned body with a flat reflection plane on one side. This scheme simulates a two-body configuration and saves computational time and storage.

A "wire frame" of the computational multiblock region with the embedded surface grid generated on the finned-body configuration is shown in Fig. 3a. A closeup of this body surface grid is presented in Fig. 3b. The body surface is covered with a 101×13 grid and each fin surface with a 39×10 grid.

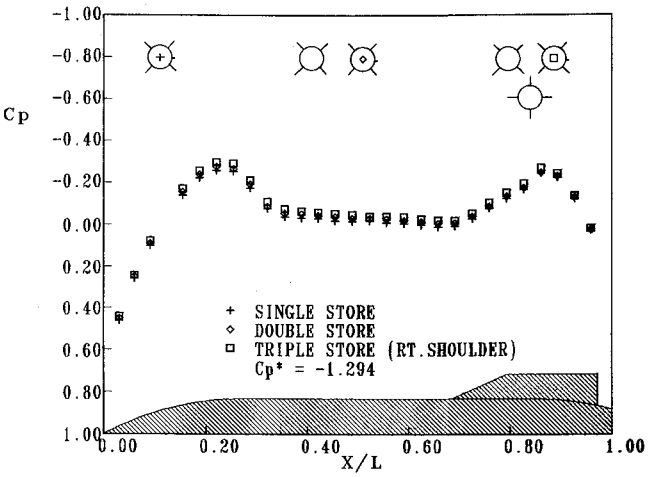

Fig. 4a Mutual interference comparison: $M_\infty = 0.60$, $\alpha = 0$ deg, $\phi = 95$ deg.

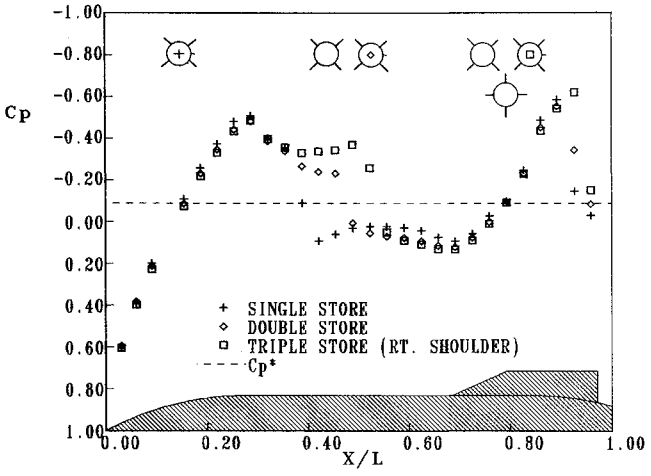

Fig. 4b Mutual interference comparison: $M_\infty = 0.95$, $\alpha = 0$ deg, $\phi = 95$ deg.

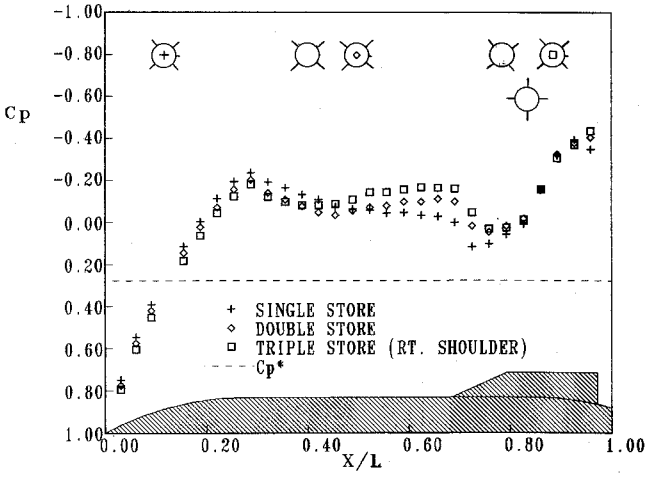

Fig. 4c Mutual interference comparison: $M_\infty = 1.20$, $\alpha = 0$ deg, $\phi = 95$ deg.

Results and Discussion

The effect of Mach number and configuration variations on the mutual aerodynamic interference occurring around the bodies are presented in Figs. 4a–4c for $\alpha = 0$ deg and an outboard circumferential location of $\phi = 95$ deg. The fins are in the x orientation. As demonstrated by the close agreement with the single-store data in Fig. 4a, there is little mutual interference for the two- and three-body combinations at $M_\infty = 0.60$. The presence of mutual interference is evident at

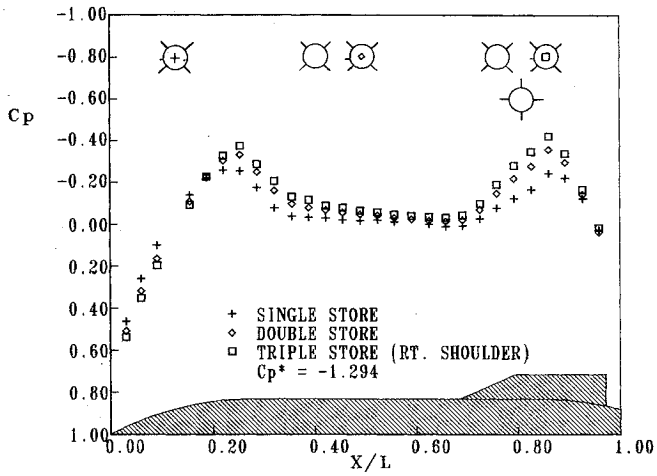

Fig. 5a Mutual interference comparison: $M_\infty = 0.60$, $\alpha = 0$ deg, $\phi = 265$ deg.

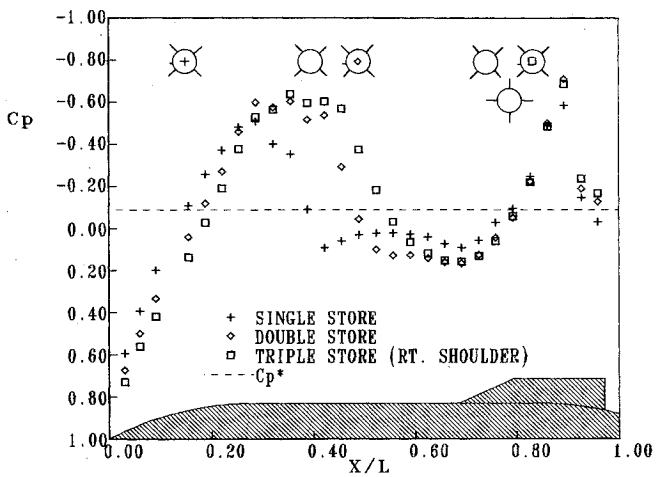

Fig. 5b Mutual interference comparison: $M_\infty = 0.95$, $\alpha = 0$ deg, $\phi = 265$ deg.

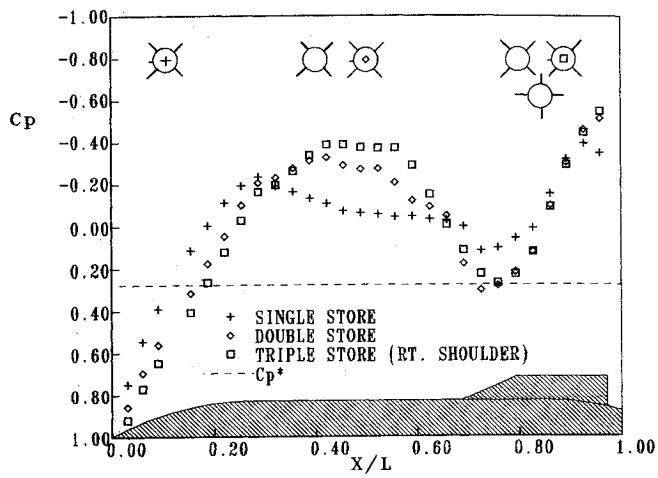

Fig. 5c Mutual interference comparison: $M_\infty = 1.20$, $\alpha = 0$ deg, $\phi = 265$ deg.

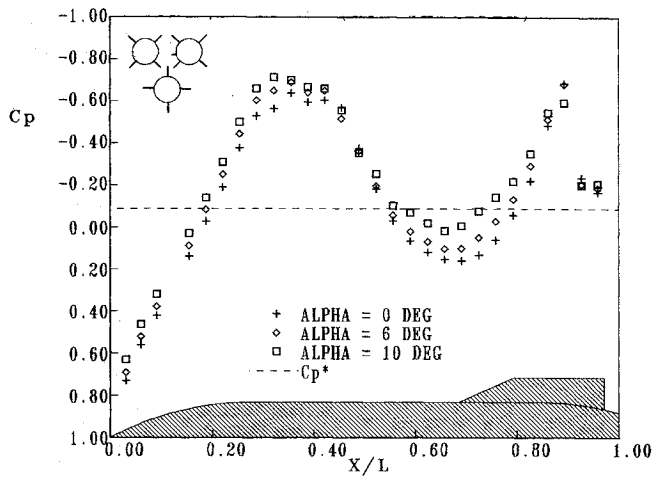

Fig. 6 Inboard body pressure as a function of incidence: $M_\infty = 0.95$, $\phi = 265$ deg.

$M_\infty = 0.95$ in the cylindrical region of the body, approximately midway between the shoulder and the start of the fin root (Fig. 4b). The existence of this mutual interference corresponds primarily to an increase in the length of the supersonic region for the multiple-store cases. The presence of a second store pushes the shock farther back on the body, and the addition of a third store pushes it back even further. Figure 4c shows that there is little mutual interference along this outboard meridian at $M_\infty = 1.20$. What interference exists commences near the middle of the cylinder and terminates near the aft ogive juncture where the flow undergoes an expansion. These results are very similar to those reported in Ref. 5 for these same configurations without fins. This demonstrates that the influence of these fins one body pressures at this outboard meridian is negligible.

The effects of Mach number and configuration variations for an inboard circumferential location denoted at $\phi = 265$ deg ($\alpha = 0$ deg) are shown in Figs. 5a-5c. The amount of interference present at $M_\infty = 0.60$ for this inboard location (Fig. 5a), though small, is somewhat greater than that experienced at the $\phi = 95$ deg position. This is also in keeping with the results of the unfinned stores[5] that demonstrated, not surprisingly, that the inboard region of a store is the region most influenced by the proximity of the other store(s). However, the multibody interference demonstrated for $M_\infty = 0.95$ at this inboard location (Fig. 5b) is substantially greater than the corresponding interference at an outbord position (Fig. 4b). The shocks appear to be stronger and occur at about the same midbody locations as on the outboard surfaces. Figure 5c demonstrates the extent of mutual interference at $M_\infty = 1.20$ along an inboard ($\phi = 265$ deg) meridian. As was the case with the unfinned results,[5] the interference begins at the nose tip and is more significant than at the outboard position. It was noted in Ref. 5 that this interference in the nose region may be due to the bow shock being pushed further upstream due to an increase in configuration cross-section area as additional stores are added.

As was the case with the outboard results, the inboard body pressure data of these finned (x-configured) stores closely match those of the unfinned configurations.

Figure 6 shows how the pressure along an inboard body region of the x-fin triple-store configuration varies as a function of angle of attack for $M_\infty = 0.95$. An inboard location ($\phi = 265$ deg) on the right shoulder store was chosen for comparison. The experimental data indicate that there is a small variation in pressure along the length of the body as the incidence of the configuration is increased from $\alpha = 0$ to 10 deg. This tends to indicate that the magnitude of multibody interference is influenced more by the presence of additional stores than by the angle of configuration incidence, provided that the angle is 10 deg or less.

Figures 7a-7c show the effect of Mach number on mutual interference occurring along a local chord on a + configured fin at $\phi_f = 270$ deg, $\alpha = 0$ deg, and 80% fin span (η). Figure 7a demonstrates that there is substantial multibody interference on this portion of the fin at $M_\infty = 0.60$. However, there appears to be little difference in the amount of mutual interference on the fin regarding the two- and three-store con-

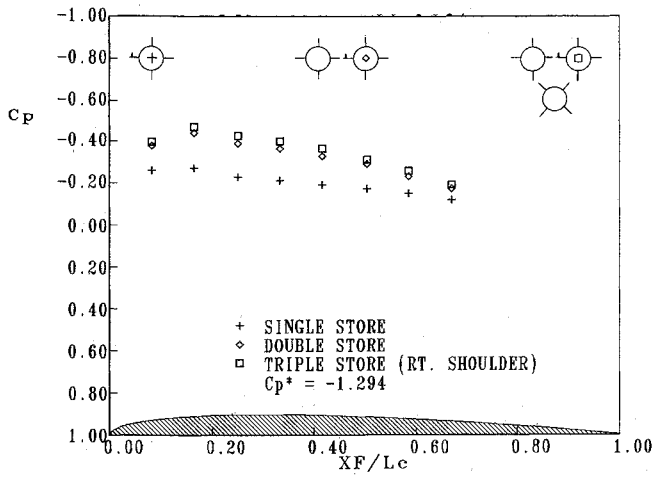

Fig. 7a Mutual interference comparison: $M_\infty = 0.60$, $\alpha = 0$ deg, $\phi_f = 270$ deg, $\eta = 0.80$.

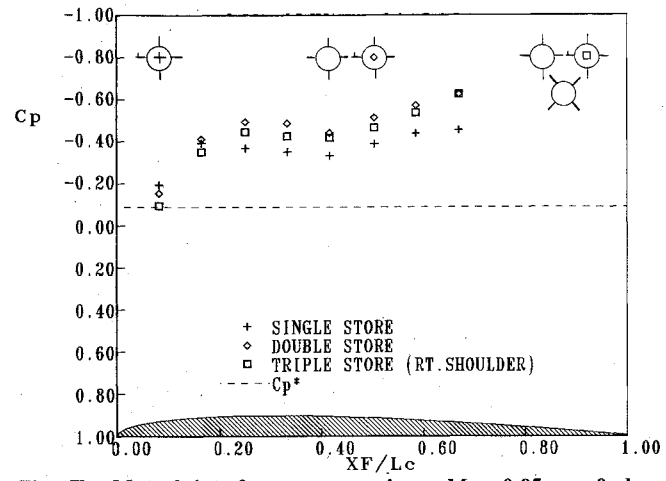

Fig. 7b Mutual interference comparison: $M_\infty = 0.95$, $\alpha = 0$ deg, $\phi_f = 270$ deg, $\eta = 0.80$.

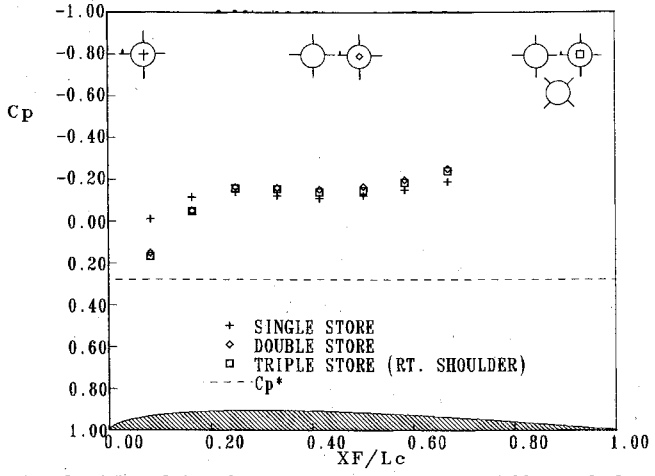

Fig. 7c Mutual interference comparison: $M_\infty = 1.20$, $\alpha = 0$ deg, $\phi_f = 270$ deg, $\eta = 0.80$.

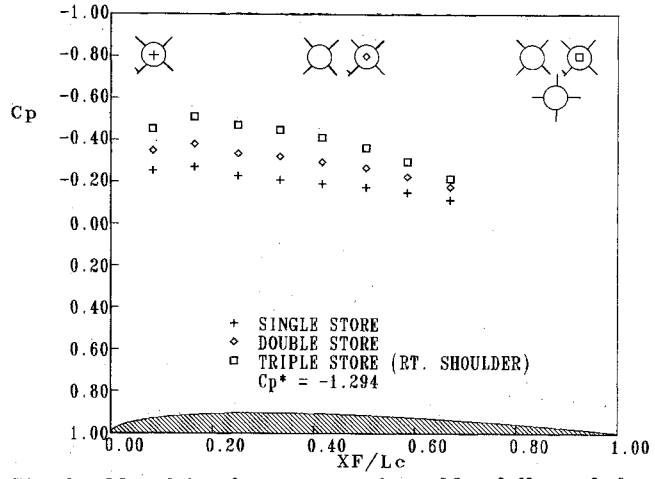

Fig. 8a Mutual interference comparison: $M_\infty = 0.60$, $\alpha = 0$ deg, $\phi_f = 225$ deg, $\eta = 0.80$.

figurations. This is probably due to the blocking effect of the fin with respect to the aerodynamic influence of the bottom store. Figure 7b shows the mutual interference on the fin at $M_\infty = 0.95$. From $XF/L_c \simeq 0.20$ aft, there appears to be slightly more interference generated by the double configuration than by the triple configuration. The reason for this is not clearly understood. However, the magnitude of the mutual interference is small for both the double- and triple-store configurations. A similar phenomenon is shown in Fig. 7c for $M_\infty = 1.20$. Except near the leading edge, there is even less interference generated by the presence of additional stores. As with the $M_\infty = 0.95$ case (Fig. 7b), the flow along this local chord is entirely supersonic. It seems that the effect of supersonic flow on the fin tends to minimize the influence of the additional bodies in the multistore configurations. Figures 8a–8c show the effect of Mach number on mutual interference occurring along a local chord on an x-configured fin at $\phi_f = 225$ deg and 80% fin span ($\alpha = 0$ deg). As with the + orientation (Fig. 7a), Fig. 8a demonstrates significant multibody interference at this spanwise location for $M_\infty = 0.60$. The x-configured fin arrangement appears to generate greater mutual interference with regard to the triple configuration than did the + alignment. This is to be expected since the x fin, triple-store alignment blocks the influence of the bottom store less than does the + fin configuration. Figure 8b shows the mutual interference on the fin at $M_\infty = 0.95$. There appears to be only a slight difference in the amount of multibody interference experienced by the fin on the double as opposed to the triple configuration. The pressure profiles are somewhat similar to those of the corresponding + configurations. However, unlike the + configurations, the x-oriented fin data show that there is slightly more interference associated with the triple configuration than for the two-store case at this Mach number. The mutual interference on the x-oriented fins at $M_\infty = 1.20$ is shown in Fig. 8c. There is evidence of some mutual interference in the vicinity of the leading edge and aft to approximately 30% of the local chord. Multiple-body interference is negligible from that region to where the pressure taps end at $XF/L_c \simeq 0.67$.

Figures 9a and 9b show how the pressure along an inboard fin varies as a function of angle of attack for the + and x-configured triple-store configurations, respectively. Figure 9a shows the effect of angle of attack on a local chordwise pressure distribution of the leeward fin surface on the right shoulder store ($\phi_f = 270$ deg). The decrease in pressure is significant as the configuration is pitched from 0 to 10 deg. This variation in fin pressure is much greater than that due to the interference of multiple bodies at zero incidence (Fig. 7b). Results are presented in Fig. 9b for the x-configured fin at $\phi_f = 225$ deg. Note that the pressure variation along the x-oriented inboard fin is not as pronounced, probably owing to the relative blocking effects of the two fin orientations discussed earlier. Here, too, the pressure variation is greater than that due to the addition of stores to the configuration (Fig. 8b). When compared to the body pressure data of Fig. 6, it is evident that the fins are more sensitive to angle-of-attack variation than is the body in this inboard region of maximum interference.

Figure 10a illustrates how mutual interference varies as a function of fin span for the triple-store (+ fin) configuration

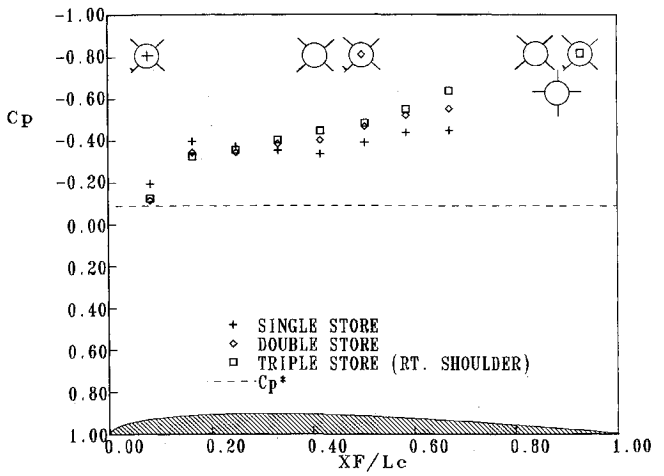

Fig. 8b Mutual interference comparison: $M_\infty = 0.95$, $\alpha = 0$ deg, $\phi_f = 225$ deg, $\eta = 0.80$.

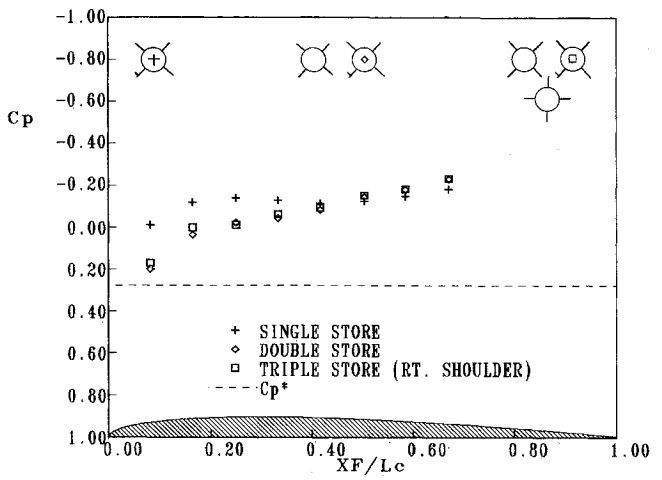

Fig. 8c Mutual interference comparison: $M_\infty = 1.20$, $\alpha = 0$ deg, $\phi_f = 225$ deg, $\eta = 0.80$.

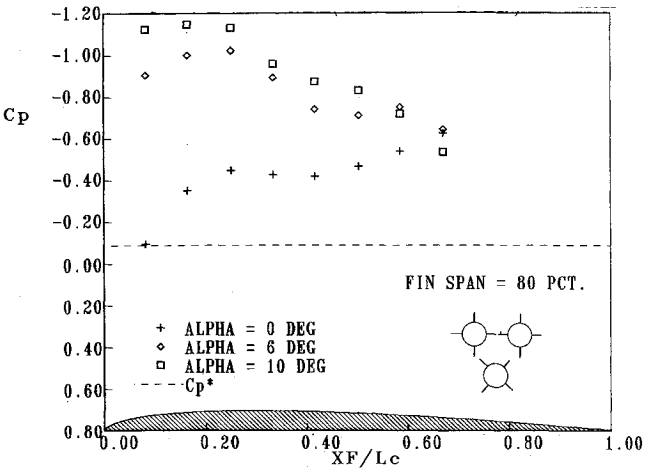

Fig. 9a Plus-configured fin lee-side pressure as a function of incidence: $M_\infty = 0.95$, $\phi_f = 270$ deg.

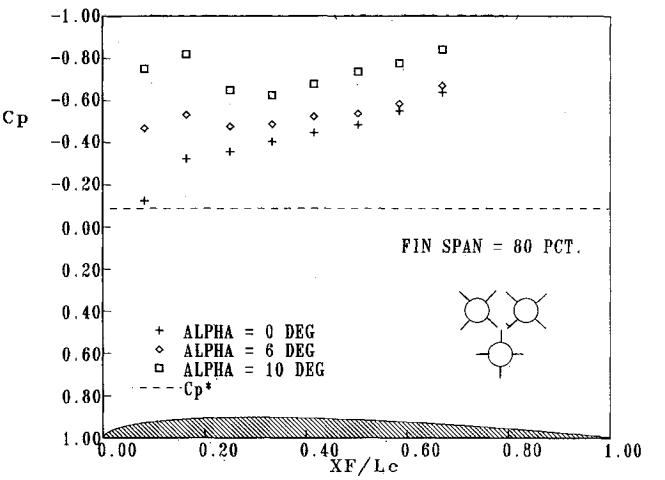

Fig. 9b *X*-configured fin lee-side pressure as a function of incidence: $M_\infty = 0.95$, $\phi_f = 225$ deg.

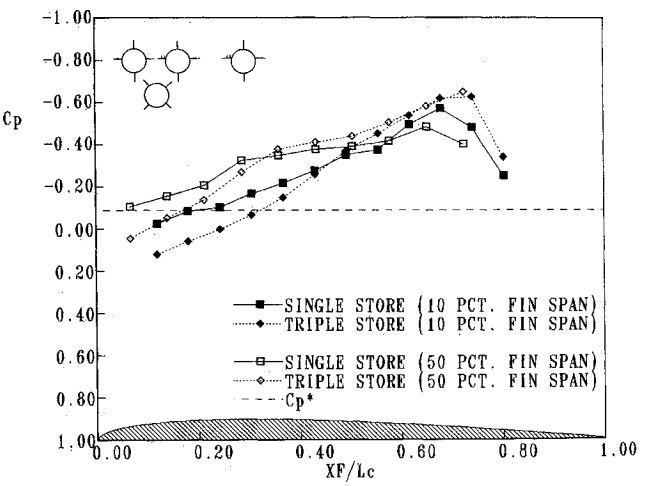

Fig. 10a Spanwise comparison of triple-store (+ fin) interference: $M_\infty = 0.95$, $\alpha = 0$ deg.

at $M_\infty = 0.95$, $\alpha = 0$ deg. The data indicate that considerable interference exists at $X/L \simeq 50\%$ and aft along the local chord beginning at $XF/L_c \simeq 0.65$. Because of model pressure tap limitations, it is not clear how far aft this region of interference extends. However, an examination of the oil flow pictures of the single-store (Fig. 10b) and the triple-store configuration (Fig. 10c) may provide additional insight. On the single store (Fig. 10b), there is evidence of a vortical flow forming in the middle of the fin beginning at $XF/L_c \simeq 0.70$ and extending to $XF/L_c \simeq 0.85$. This vortical flow seems to dissipate on the inboard fins of the triple-store configuration, but remains on the outboard fins where mutual interference is small (Fig. 10c). The dissipation of this vortical flow on the triple-store configuration may be the result of an increase in interference occurring in this region of the inboard fins and a corresponding higher local Mach number. This is further substantiated by the fact that oil flow photographs at freestream Mach numbers greater than 0.95 do not exhibit a vortical flow pattern on the fins for any configuration.

Figures 11a and 11b illustrate typical Euler solver results for the double-store (*x*-fin) configuration at $M_\infty = 0.95$, $\alpha = 0$ deg. Figure 11a shows excellent agreement with the experimental data along the length of the body at both an outboard ($\phi = 95$ deg) and an inboard ($\phi = 265$ deg) location. Only near $X/L = 0.9$ does the prediction significantly differ from the data. This region corresponds to the vortical flow on the fin and may be a direct result. Figure 11b demonstrates the comparison along both an outboard fin ($\phi_f = 45$ deg) and an inboard fin ($\phi_f = 315$ deg) at $\eta = 80\%$. Here, too, the correlation between the numerical and experimental data is very good except near the leading edge of both fins. This may be due to the grid cell sizing in this region of large pressure gradients. Figure 11c shows the oil flow photograph of this configuration at $M_\infty = 0.95$, $\alpha = 0$ deg. The migration of the skin friction lines to the inboard sides of the bodies indicates a significantly lower pressure in the region between the stores. This contention is supported by comparing the two curves in Fig. 11a. Between the stores at $\phi = 265$ deg, the expansion peak is significantly higher than at $\phi = 95$ deg, resulting in a lower pressure

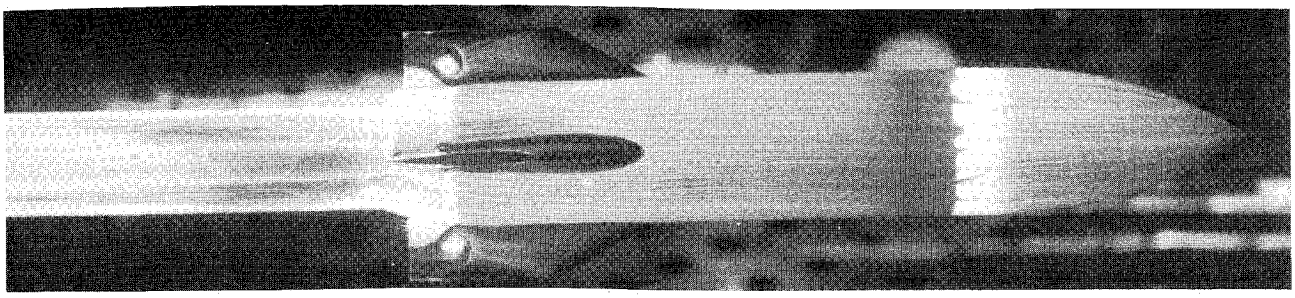

Fig. 10b Single-store (+ fin) oil flow: $M_\infty = 0.95$, $\alpha = 0$ deg.

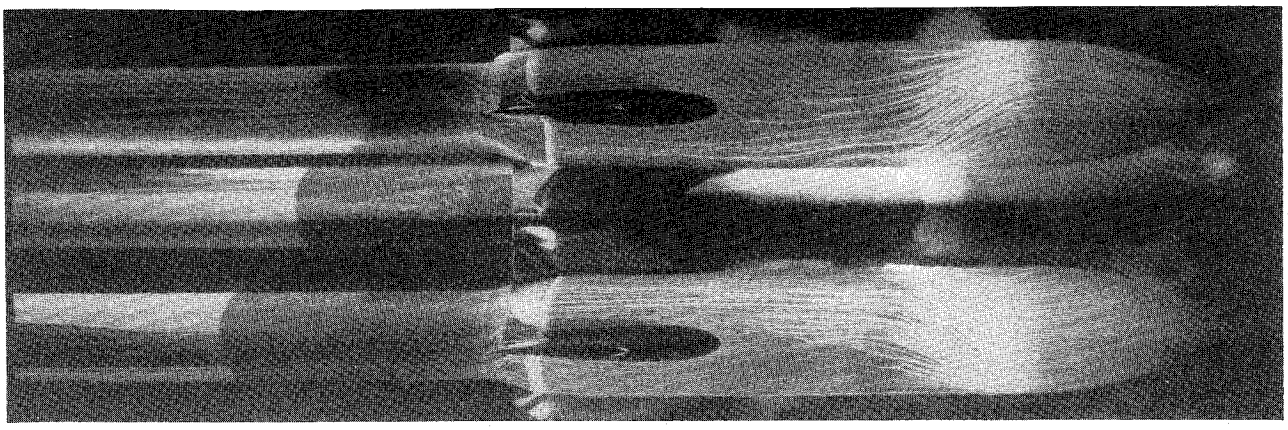

Fig. 10c Triple-store (+ fin) oil flow: $M_\infty = 0.95$, $\alpha = 0$ deg.

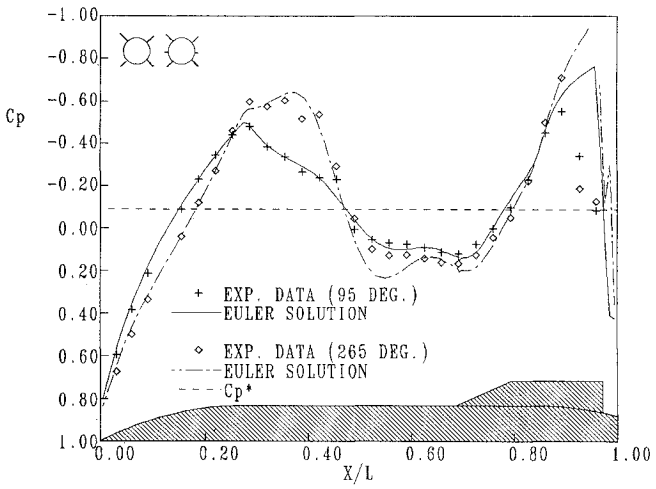

Fig. 11a Double-store (body) experimental and numerical comparison: $M_\infty = 0.95$, $\alpha = 0$ deg.

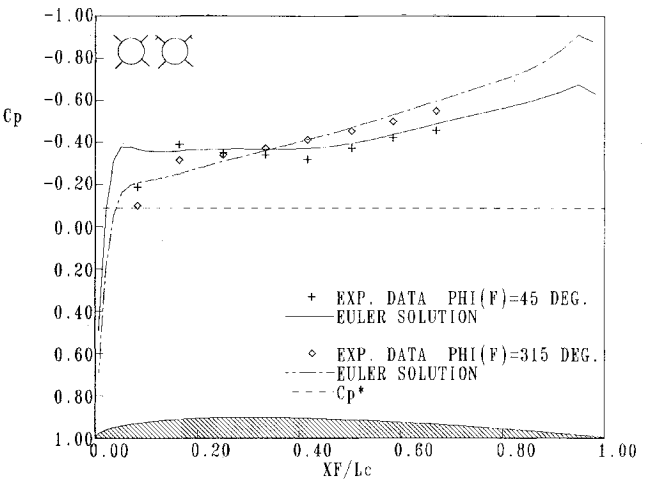

Fig. 11b Double-store (fin) experimental and numerical comparison: $M_\infty = 0.95$, $\alpha = 0$ deg, $\eta = 0.80$.

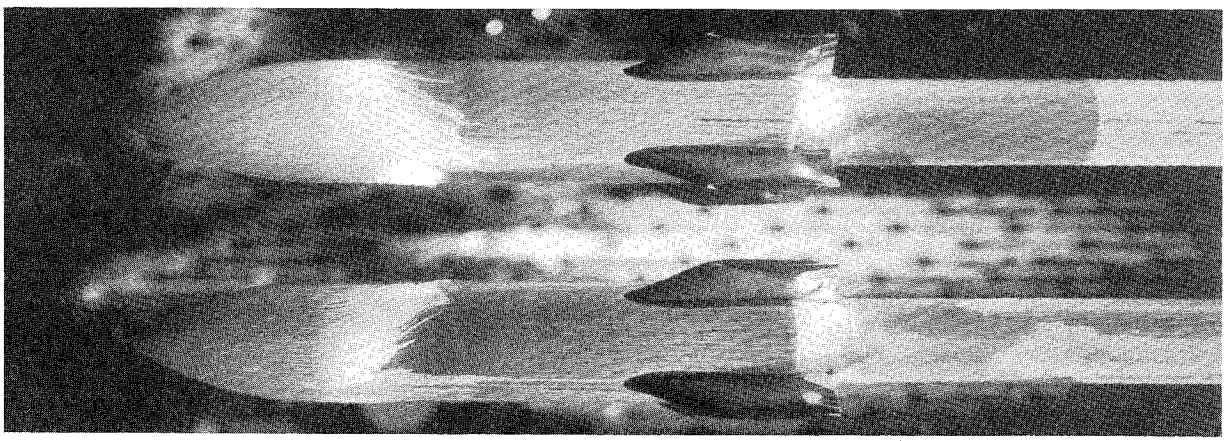

Fig. 11c Double-store (x-fin) oil flow: $M_\infty = 0.95$, $\alpha = 0$ deg.

area between the stores. The two stores tend to act as a nozzle in accelerating the flow and lowering the pressure.

Concluding Remarks

A study of finned, multibody aerodynamic interference based on recently obtained experimental data and computational fluid dynamics prediction has been performed. Several general conclusions can be made based on the results of this investigation.

The mutual aerodynamic interference characteristics of multiple, finned bodies are similar to those of multiple, unfinned bodies. As with the unfinned stores of Ref. 5, the magnitude of the body interference seems to be less a function of configuration angle of attack than of freestream Mach number and the proximity of other bodies.

Finned, multibody interference (measured on the body) in the transonic region seems to be greatest at Mach numbers near 1. As was the case with the unfinned stores, this interference subsides as the freestream Mach number increases or deceases from sonic conditions. However, the interference on the inboard fins shows the opposite tendency. These fins seem to experience greater multibody interference at lower Mach numbers than at Mach numbers closer to 1. The magnitude of this fin interference is somewhat dependent on the fin roll attitude and the resulting blocking effects. For this reason, the triple-configuration, x-oriented fin arrangement generates more mutual interference than does the corresponding + fin alignment. Futhermore, in the inboard region of maximum interference, both fin roll orientations are significantly more sensitive to angle-of-attack variation than is the body surface.

Finally, it is recognized that multibody interference would increase (particularly in the inboard regions) if a pylon or rack were added to the configuration. Such an addition would increase the viscous effects. As a consequence, the Euler flow solver might provide a less accurate solution. However, it was concluded that a Euler flow solver can provide accurate predictions of finned, multibody interference as long as an appropriate grid is used and the viscous effects associated with these configurations remain small.

References

[1]Lijewski, L.E., Thompson, J.F., and Whitfield, D.L., "Computational Fluid Dynamics for Weapon Carriage and Separation," AGARD Symposium on Store Airframe Aerodynamics, Paper No. 3, Oct. 1985.

[2]Belk, D.M., Janus, M.J., and Whitfield, D.L., "The Three-Dimensional Unsteady Euler Equations Solutions on Dynamic Grids," AIAA Paper 85-1704, July 1985.

[3]Dougherty, F.C., Benek, J.A., and Steger, J.L., "On Application of Chimera Grid Schemes to Store Separation," NASA TM 881193, Oct. 1985.

[4]Janus, J.M., "The Development of a Three-Dimensional Split Flux Vector Euler Solver with Dynamic Grid Applications," M.S. Thesis, Mississippi State Univ., Mississippi State, MS, Aug. 1984.

[5]Cottrell, C.J., Martinez, A., and Chapman, G.T., "A Study of Multi-Body Aerodynamic Interference at Transonic Mach Numbers," AIAA Paper 87-0519, Jan. 1987.

[6]Goodwin, F.K. and Neilsen, J.N., "Experimental and Theoretical Study of Flowfields and Store Forces in Close Proximity to a Triple Ejection Rack at Transonic Speeds," Naval Weapons Center, TP-6210, Sept. 1980.

[7]Belk, D.M. and Whitfield, D.L., "Three-Dimensional Euler Solutions on Blocked Grids Using an Implicit Two-Pass Algorithm," AIAA Paper 87-0450, Jan. 1987.

[8]Whitfield, D.L., "Implicit Upwind Finite Volume Scheme for the Three-Dimensional Euler Equations," Mississippi State Univ. Rept. MSSU-EIRS-ASE-85-1, Mississippi, State, MS, Sept. 1985.

[9]Whitfield, D.L. and Janus, J.M., "Three-Dimensional Unsteady Euler Equations Solution Using Flux Vector Splitting," AIAA Paper 84-1552, June 1984.

[10]Thompson, J.F. and Warsi, Z.U.A., "Three-Dimensional Grid Generation from Elliptic Systems," AIAA Paper 83-1905, July 1983.